NEUROSCIENCE

Dendritic action potentials and computation in human layer 2/3 cortical neurons

Albert Gidon[1], Timothy Adam Zolnik[1], Pawel Fidzinski[2,3], Felix Bolduan[4], Athanasia Papoutsi[5], Panayiota Poirazi[5], Martin Holtkamp[2], Imre Vida[3,4], Matthew Evan Larkum[1,3]*

The active electrical properties of dendrites shape neuronal input and output and are fundamental to brain function. However, our knowledge of active dendrites has been almost entirely acquired from studies of rodents. In this work, we investigated the dendrites of layer 2 and 3 (L2/3) pyramidal neurons of the human cerebral cortex ex vivo. In these neurons, we discovered a class of calcium-mediated dendritic action potentials (dCaAPs) whose waveform and effects on neuronal output have not been previously described. In contrast to typical all-or-none action potentials, dCaAPs were graded; their amplitudes were maximal for threshold-level stimuli but dampened for stronger stimuli. These dCaAPs enabled the dendrites of individual human neocortical pyramidal neurons to classify linearly nonseparable inputs—a computation conventionally thought to require multilayered networks.

The expansion of the human brain during evolution led to an extraordinarily thick cortex (~3 mm), which is disproportionately thickened in layers 2 and 3 (L2/3) (1). Consequently, human cortical neurons of L2/3 constitute large and elaborate dendritic trees (2, 3), decorated by numerous synaptic inputs (1). The active electrical properties of these dendrites largely determine the repertoire of transformations of the synaptic inputs to axonal action potentials (APs) at the output. Thus, they constitute a key element of the neuron's computational power.

We used dual somatodendritic patch clamp recordings and two-photon imaging to directly investigate the active properties of L2/3 dendrites in acute slices from surgically resected brain tissue of the human neocortex from epilepsy and tumor patients. Subthreshold (steady-state) potentials attenuated from the dendrite to the soma with a length constant (λ_{steady}) of 195 μm (fig. S1; n = 23 cells). In the opposite direction, the back-propagating action potentials (bAPs) attenuated from the soma to the dendrite with a λ_{bAP} of 290 μm (Fig. 1, A to C; n = 31 cells). Both λ_{bAP} and λ_{steady} were shorter than the length of the apical dendrite (the somata of these cells were located ~850 μm below the pia mater, on average, and the apical dendrite extended up to layer 1), which implies that strong attenuation governs the electrical activity to and from most synapses located on the apical dendrite.

We filled cells with the calcium indicator Oregon-green BAPTA-1 (100 μM) and measured the change in fluorescence ($\Delta F/F$) under a two-photon microscope while triggering APs at the soma. Trains of somatic APs (10 APs) at 50 Hz failed to cause Ca^{2+} influx at distal apical dendrites (fig. S2). AP trains with a higher frequency (10 APs at 200 Hz) did invade most of the apical dendrite, similarly to what has been shown previously in rodent L2/3 pyramidal neurons (4). However, these high-frequency signals were substantially attenuated at distal tuft dendrites (fig. S2). Furthermore, Ca^{2+} influx in spines was similar to that in the nearby dendritic branches, regardless of the somatic AP frequency (fig. S2D).

We next examined whether human L2/3 dendrites have intrinsic mechanisms to compensate for the large dendritic attenuation. We injected a current step into the dendrite (I_{dend}) and recorded the membrane potentials at both the dendrite and at the soma. At the soma and at the proximal dendritic sites (170 μm from the soma, on average), a suprathreshold current readily evoked somatic APs, which back-propagated into the dendrite (Fig. 1, A and B, and fig. S5H). However, when the dendritic electrode was positioned more distally, suprathreshold stimuli often evoked trains of repetitive APs that were initiated exclusively in the dendrite (Fig. 1D; for transient stimulus, see fig. S10). These results imply that L2/3 dendrites in human cortical pyramidal neurons are distinctly more excitable than the homolog dendrites in rodents, where similar steady currents evoke, at most, only a single dendritic AP at the beginning of the voltage response (5). In contrast to L2/3 pyramidal neurons, layer 5 pyramidal neurons of the human neocortex were recently reported to have reduced dendritic excitability compared with their homolog neurons in rodents (6).

High-frequency dendritic APs (>200 Hz) that were uncoupled from somatic firing have

been observed in rodent dendrites in vivo (7, 8). The authors of these studies have attributed these spikes to dendritic voltage-gated Na^+ channels and/or N-methyl-D-aspartate (NMDA) receptors. The dendritic APs in human L2/3 neurons were not blocked by the sodium channel blocker tetrodotoxin (1 μM; n = 4 cells; fig. S3), but they were abolished by the Ca^{2+} channel blocker Cd^{2+} (200 μM; n = 5 cells; fig. S3). The dendritic Ca^{2+} APs that we observed in human L2/3 neurons have not been described in the cortical neurons of other mammalian species. Dendritic APs that are mediated (or are assumed to be mediated) by sodium currents in rodents' neurons have been variously named dendritic spikes (9), prepotentials (10), Na-dSpikes (11), and dendritic action potentials (DAPs) (8). To distinguish the dendritic APs that we found in the human dendrites from those described previously, we refer to them as dendritic Ca^{2+} APs (dCaAPs).

dCaAPs were present not only in neurons from the temporal lobe of epilepsy patients but also in neurons from other neocortical areas of tumor patients (n = 4 cells from 3 patients; fig. S4). This suggests that dCaAPs are neither regionally confined nor related to pathology.

The waveform of dCaAPs was stereotypical and easily distinguished from that of bAPs. dCaAPs were typically wider than bAPs (with widths of 4.4 ± 1.4 ms, ranging between 2.6 and 8.0 ms; n = 32 cells), they were slow rising, and they did not have a kink at onset (7) (Fig. 1D). The majority of the cells (27 of 39) showed a train of (two or more) dCaAPs with a mean firing rate of 4.6 ± 1.7 Hz (dCaAPs per second). In the remaining 12 dendrites, a single dCaAP was triggered immediately after the beginning of the stimulus. Unlike the bAP (Fig. 1C), the amplitude of the dCaAPs (Fig. 1E) and their upstroke (fig. S5) were not dependent on the distance from the soma (average dCaAP amplitude 43.8 ± 13.8 mV, ranging between 13.0 and 67.0 mV; n = 32 cells, measured at threshold). This is consistent with both variability of the dCaAP initiation site and variability of dCaAP properties (for further details, see figs. S5 and S11). We never detected high-amplitude, long-duration, Ca^{2+}-mediated plateau potentials, which are common in the apical dendrites of L5 neurons in rodents.

The impact of dCaAPs on the soma was variable. In some of the cells (17 of 37), the dCaAPs were coupled with somatic APs (coupled dCaAPs; e.g., Fig. 1F). Unlike forward-propagating dendritic APs in other pyramidal neurons (12–14), coupled dCaAPs triggered somatic APs immediately and/or with a delay ranging between 21.6 and 116.9 ms (53.8 ± 26.8 ms, on average, in 11 out of 17 coupled cells; Fig. 1, F and G, and fig. S6). Coupled dCaAPs that triggered somatic APs with a delay were classified as complex.
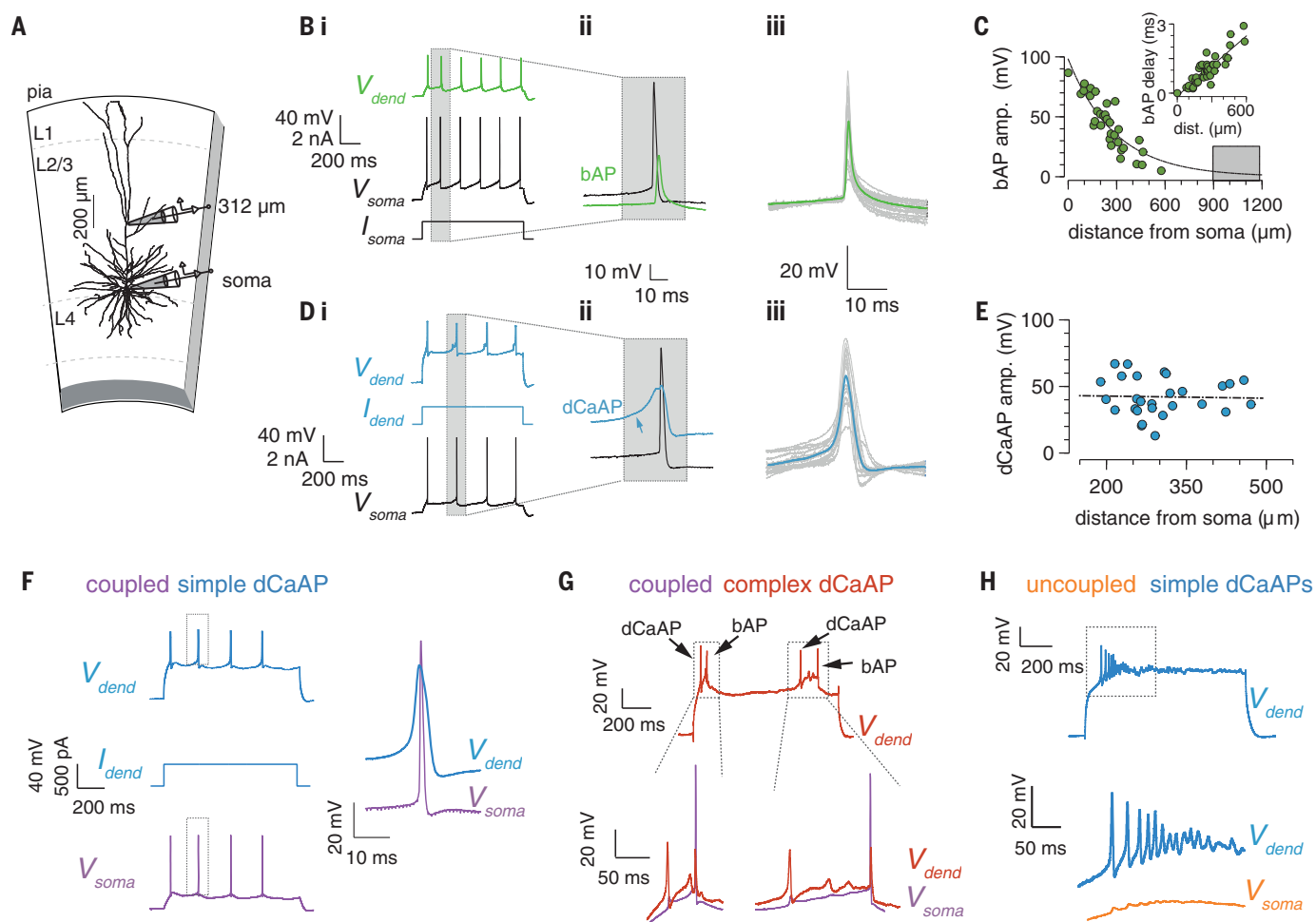
Fig. 1. bAPs and dCaAPs in human dendrites of L2/3 neurons.
(**A**) Experimental setting: L2/3 neuron at a depth of 1130 μm below the pial surface, with a somatic electrode and a dendritic electrode placed at 312 μm from the soma. (**B**) (i) Recordings from the cell in (A). bAPs in green (V_{dend}) and corresponding somatic APs in black (V_{soma}) triggered by somatic current injection (I_{soma}) are shown. (ii) Somatic AP preceded the bAP [magnified from the frame in (i)]. (iii) bAPs in 16 dendrites (gray) and their average (green) aligned to their peak. (**C**) bAP amplitude (green dots) and exponential fit (length constant λ_{bAP} = 290 μm; n = 31 cells; dashed line) against distance from the soma. Gray area indicates the putative tuft region in layer 1 for the longest dendrite. (Inset) Delay of the bAP peak against distance from the soma with linear fit (r^2 = 0.78, where r^2 is the coefficient of determination). amp., amplitude; dist., distance. (**D**) (i) dCaAPs (V_{dend}; blue) triggered by a square current injected at the dendrite (I_{dend}) and the resulting somatic AP (black) from the cell in (A). (ii) Somatic AP (in black) and a dCaAP (in blue) magnified from (i). The slow rising dCaAP (blue arrow) precedes the somatic AP. (iii) Initial dCaAP in each recording at threshold in the same 16 dendrites (gray) in (iii) of (B) and their average trace (blue) aligned to their peak. (**E**) dCaAP amplitude is independent of the distance from the soma (n = 28 cells). Linear fit is shown with the dashed line (r^2 = 0.0009). (**F**) (Left) Coupled and simple dCaAPs (blue trace) and somatic APs (purple trace) triggered by I_{dend}. (Right) Magnified dCaAP (in blue) and a somatic AP (in purple) framed in the traces on the left are shown. (**G**) (Top) Two coupled and complex dCaAPs (in red) triggered delayed somatic APs [in purple, magnified at (bottom)]. (**H**) Burst of simple and uncoupled dCaAPs in blue (top) with somatic APs (bottom).

Without exception, each coupled dCaAP triggered a single somatic AP, which implies that, unlike calcium APs in the dendrites of other neurons (*15, 16*), dCaAPs did not induce bursts of somatic APs. In the other 20 cells, dCaAPs were uncoupled. They were confined to the apical dendrite, unable to evoke somatic APs. Typically, uncoupled dCaAPs were observed in more distal dendritic recording sites (335 ± 113 μm from the soma) than the coupled dCaAPs that triggered somatic APs (265 ± 71 μm from the soma), but the distance difference was not statistically significant (Wilcoxon rank sum test, P = 0.077). Additionally, one coupled and three uncoupled cells fired bursts of three or more dCaAPs at the beginning of the stimulus (28 to 73 Hz). In fig. S7, we summarize the classification of the dCaAPs on the basis of their ability to trigger APs at the soma (i.e., coupled versus uncoupled) and their complexity (i.e., complex and/or simple). Most of the dendrites with complex dCaAPs also triggered simple dCaAPs, suggesting that their behavior might be activity- or input-dependent and/or modulated by other factors (*17*).

dCaAPs affected the input–output transformation of the cells. Typically, somatic AP firing increases with the input current intensity injected to the soma. In contrast, in 4 cells (out of 12 cells that had repetitive and coupled dCaAPs) our recordings revealed an inverse behavior where increasing the intensity of dendritic (rather than somatic) current injection resulted in decreased somatic firing. For example, in Fig. 2, A and B, the dendritic electrode evoked one or two somatic APs with current near threshold but failed to evoke APs for higher current intensity. In contrast, at the
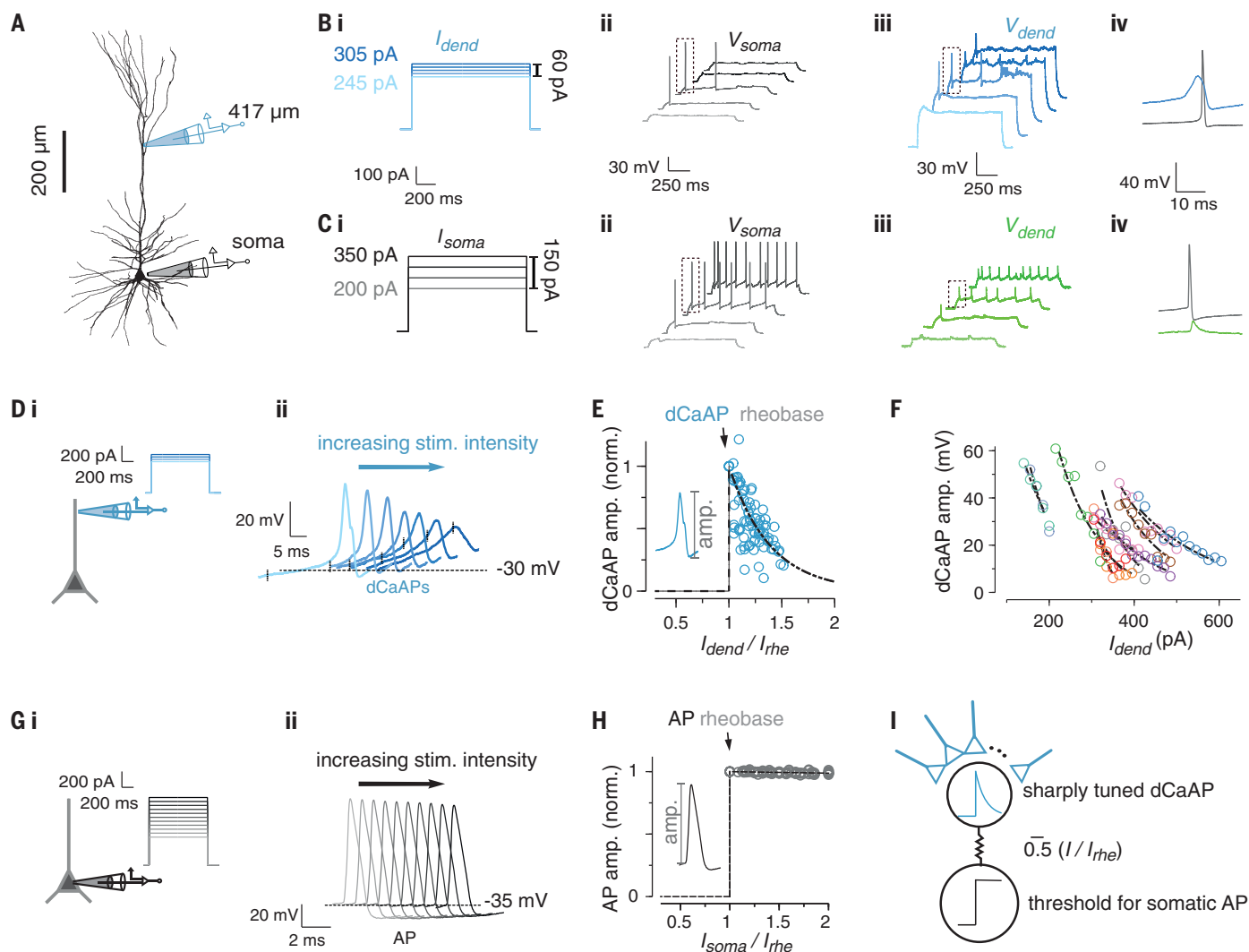
Fig. 2. dCaAPs are sharply tuned to the stimulus intensity. (**A**) L2/3 pyramidal neuron with soma 886 μm below the pia. The somatic and dendritic electrodes are shown in black and blue, respectively. Recordings from this cell are shown in (B) and (C). (**B**) Dendritic current (I_{dend}) injected 417 μm from the soma (i) and corresponding somatic (ii) and dendritic traces (iii). (ii) I_{dend} of 260 and 275 pA, but neither smaller nor larger current, resulted in somatic APs. (iii) dCaAP amplitudes were maximal for I_{dend} of 260 and 275 pA, whereas $I_{dend} > 275$ pA dampened them. (iv) dCaAP (in blue) precedes the somatic AP (in gray); traces are magnified from the framed APs in (ii) and (iii). (**C**) Somatic current injection, I_{soma} (i), somatic AP trains (ii), and bAP (iii) for similar ranges of current intensity as those shown in (i) of (B). (iv) Somatic AP (in gray) precedes the dendritic bAP (in green); traces are magnified from the framed APs in (ii) and (iii). (**D**)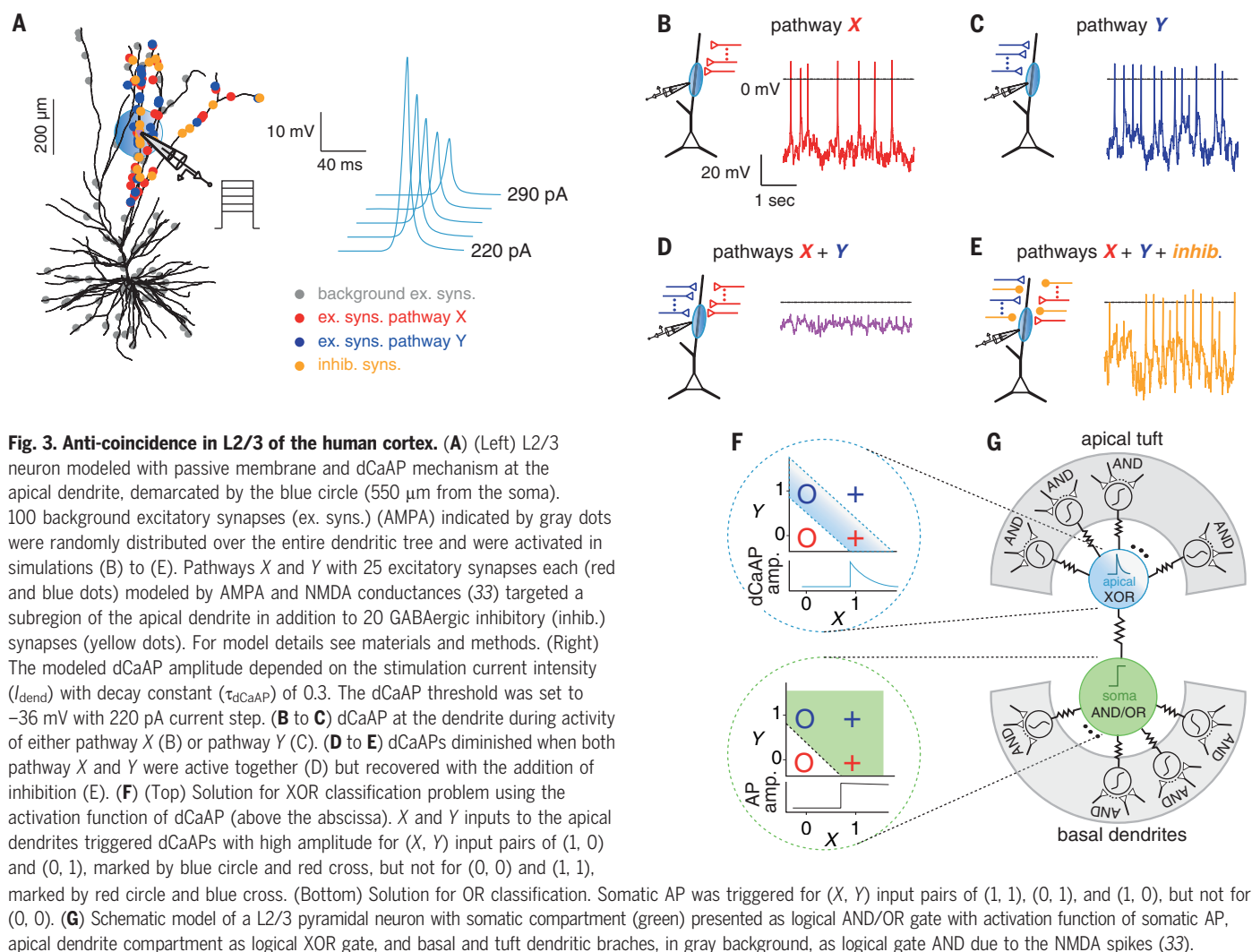 Increase in I_{dend} (i) dampened the dCaAPs' amplitude (ii); vertical tick on each trace marks 50 ms after I_{dend} onset. stim., stimulation; norm., normalized. (**E**) Amplitude of the first dCaAP in each trace against I_{dend} normalized by rheobase (I_{rhe}) for uncoupled dCaAPs (12 dendrites) and exponential fit (dashed line), with a decay constant (τ_{dCaAP}) of 0.39 (median 0.38) in units of rheobase. (**F**) dCaAP amplitudes as in (E) but not normalized by I_{rhe}. Dots in different colors represent dCaAP amplitudes from different cell (12 dendrites) with exponential fit (dashed lines). (**G**) As in (D) but for somatic APs. I_{soma}, (i) and the resulting somatic APs (ii). (**H**) AP amplitude plotted against the normalized somatic input current strength (I_{soma}/I_{rhe}). The amplitude of the somatic AP was fixed and did not depend on I_{soma} for a range of stimuli strengths as in (ii) of (G) (exponential fit with $\tau_{AP} = 82$, units of somatic I_{rhe}). (**I**) Dendritic and somatic activation functions for dCaAPs (blue curve) and for somatic APs (black curve).

soma of the same cells, AP output increased with the input's strength (Fig. 2C). These results are explained by the unusual active properties of dCaAPs. dCaAPs evoked by the dendritic electrode triggered somatic APs near threshold but were suppressed by further increase in the stimulus intensity (Fig. 2B).

The dendritic activation function (namely, the amplitude of dCaAPs as a function of the intensity of the current injection in the den-drite, I_{dend}) reached its maximal value at the rheobase (i.e., for $I_{dend} = I_{rhe}$ where I_{rhe} is the threshold current for triggering a dCaAP) and decayed for stronger I_{dend} (Fig. 2, D to F; 12 uncoupled dCaAPs). The mean width of the dendritic activation function (defined here as the decay constant of a single exponential fit) was 0.39 (0.38 median; in units of I_{rhe}), which indicates that dCaAPs are sharply tuned (highly selective) to a particular input strength. Addi-tionally, L2/3 dendrites were heterogeneous in their activation function threshold and width (Fig. 2F). In contrast, in a similar range of input intensities, somatic APs (Fig. 2, G to H) showed a typical threshold activation function; once a somatic AP was triggered, its amplitude was virtually independent of the input intensity (Fig. 2H). Unlike other dendritic APs in the mammalian neocortex—namely, NMDA spikes (*18*) and dendritic Ca²⁺ APs in layer

Fig. 3. Anti-coincidence in L2/3 of the human cortex. (**A**) (Left) L2/3 neuron modeled with passive membrane and dCaAP mechanism at the apical dendrite, demarcated by the blue circle (550 μm from the soma). 100 background excitatory synapses (ex. syns.) (AMPA) indicated by gray dots were randomly distributed over the entire dendritic tree and were activated in simulations (B) to (E). Pathways *X* and *Y* with 25 excitatory synapses each (red and blue dots) modeled by AMPA and NMDA conductances (*33*) targeted a subregion of the apical dendrite in addition to 20 GABAergic inhibitory (inhib.) synapses (yellow dots). For model details see materials and methods. (Right) The modeled dCaAP amplitude depended on the stimulation current intensity (I_{dend}) with decay constant (τ_{dCaAP}) of 0.3. The dCaAP threshold was set to −36 mV with 220 pA current step. (**B** to **C**) dCaAP at the dendrite during activity of either pathway *X* (B) or pathway *Y* (C). (**D** to **E**) dCaAPs diminished when both pathway *X* and *Y* were active together (D) but recovered with the addition of inhibition (E). (**F**) (Top) Solution for XOR classification problem using the activation function of dCaAP (above the abscissa). *X* and *Y* inputs to the apical dendrites triggered dCaAPs with high amplitude for (*X*, *Y*) input pairs of (1, 0) and (0, 1), marked by blue circle and red cross, but not for (0, 0) and (1, 1), marked by red circle and blue cross. (Bottom) Solution for OR classification. Somatic AP was triggered for (*X*, *Y*) input pairs of (1, 1), (0, 1), and (1, 0), but not for (0, 0). (**G**) Schematic model of a L2/3 pyramidal neuron with somatic compartment (green) presented as logical AND/OR gate with activation function of somatic AP, apical dendrite compartment as logical XOR gate, and basal and tuft dendritic branches, in gray background, as logical gate AND due to the NMDA spikes (*33*).

5 pyramidal neurons (*15*, *19–22*)—that were previously shown to increase with the stimulus strength, the activation function of dCaAPs in L2/3 neurons was sharply tuned to a specific input strength (Fig. 2I).

We used a compartmental model of a L2/3 pyramidal neuron that replicated the phenomenology of the dCaAP behavior in the dendrite to investigate the functional outcome of the dCaAP activation function (for a biophysical model of dCaAPs, see fig. S12). L2/3 pyramidal neuron morphology was digitally reconstructed and modeled in the NEURON (*23*) simulation environment (Fig. 3A). The dCaAP's threshold, width, and amplitude as a function of the input strength were simulated by the sum of current sources with a sigmoidal shape (for details, see materials and methods and Fig. 3A, right panel). To simulate two distinct classes of inputs, pathways *X* and *Y*, we used 25 excitatory synapses for each pathway (Fig. 3A), targeting a subregion of the apical dendrite (blue and red dots in Fig. 3A). Each of these pathways was able to trigger dCaAPs by

itself (Fig. 3, B and C). Because of the activation function of the dCaAPs in our simulation, coincident activation of two synaptic input pathways diminished the dCaAP amplitude (Fig. 3D) in contrast to other dendritic APs that amplify coincident dendritic inputs (*24*) [e.g., in layer 5 pyramidal neurons in the rodent neocortex (*25*) or in CA1 neurons of the rodent hippocampus (*26*)]. Our simulation is therefore a simple and explicit demonstration of how the dendritic mechanism observed in human L2/3 pyramidal neurons computes an anticoincident function for multiple input pathways, limiting the number and/or the strength of inputs integrated in the dendrite (for impact on the cell body, see fig. S9). Inhibition (*27*, *28*) placed at the same dendritic subregion (20 GABAergic synapses), in addition to the two excitatory pathways, repolarized the membrane and recovered the amplitude of the dCaAPs [Fig. 3E; (*29*)]. These results suggest that the precise balance between excitation and inhibition is essential for the generation of dCaAPs and indicate a

counterintuitive role for inhibition in enhancing the excitability of the dendrite (see also fig. S9, C and D).

It has long been assumed that the summation of excitatory synaptic inputs at the dendrite and the output at the axon can only instantiate logical operations such as AND and OR (*30*). Traditionally, the XOR operation has been thought to require a network solution (*31*, *32*). We found that the dCaAPs' activation function allowed them to effectively compute the XOR operation in the dendrite by suppressing the amplitude of the dCaAP when the input is above the optimal strength (Fig. 2). Thus, on the basis of our results and those of previous studies (*30*, *33*), we consider a model that portrays the somatic and dendritic compartments of L2/3 neurons as a network of coupled logical operators and corresponding activation functions (Fig. 3, F and G). In this model, the XOR operation is performed in the dendrites with dCaAPs, whereas AND/OR operations are performed at the soma and at tuft and basal dendrites

with sodium and NMDA spikes, respectively (*20, 25, 34, 35*). Our findings provide insights into the physiological building blocks that constitute the algorithms of cellular function, which ultimately give rise to the cortical network behavior.

REFERENCES AND NOTES

1. J. DeFelipe, L. Alonso-Nanclares, J. I. Arellano, *J. Neurocytol.* **31**, 299–316 (2002).
2. H. Mohan *et al.*, *Cereb. Cortex* **25**, 4839–4853 (2015).
3. Y. Deitcher *et al.*, *Cereb. Cortex* **27**, 5398–5414 (2017).
4. J. Waters, M. Larkum, B. Sakmann, F. Helmchen, *J. Neurosci.* **23**, 8558–8567 (2003).
5. M. E. Larkum, J. Waters, B. Sakmann, F. Helmchen, *J. Neurosci.* **27**, 8999–9008 (2007).
6. L. Beaulieu-Laroche *et al.*, *Cell* **175**, 643–651.e14 (2018).
7. S. L. Smith, I. T. Smith, T. Branco, M. Häusser, *Nature* **503**, 115–120 (2013).
8. J. J. Moore *et al.*, *Science* **355**, eaaj1497 (2017).
9. B. Sivyer, S. R. Williams, *Nat. Neurosci.* **16**, 1848–1856 (2013).
10. S. Crochet, P. Fuentealba, I. Timofeev, M. Steriade, *Cereb. Cortex* **14**, 1110–1121 (2004).
11. Y. Kim, C.-L. Hsu, M. S. Cembrowski, B. D. Mensh, N. Spruston, *eLife* **4**, e06414 (2015).
12. M. E. Larkum, J. J. Zhu, B. Sakmann, *J. Physiol.* **533**, 447–466 (2001).
13. N. L. Golding, N. Spruston, *Neuron* **21**, 1189–1200 (1998).
14. L. M. Palmer *et al.*, *Nat. Neurosci.* **17**, 383–390 (2014).
15. M. E. Larkum, J. J. Zhu, B. Sakmann, *Nature* **398**, 338–341 (1999).
16. N. L. Golding, H. Y. Jung, T. Mickus, N. Spruston, *J. Neurosci.* **19**, 8789–8798 (1999).
17. C. Labarrera *et al.*, *Cell Rep.* **23**, 1034–1044 (2018).
18. J. Schiller, G. Major, H. J. Koester, Y. Schiller, *Nature* **404**, 285–289 (2000).
19. M. E. Larkum, K. M. M. Kaiser, B. Sakmann, *Proc. Natl. Acad. Sci. U.S.A.* **96**, 14600–14604 (1999).
20. M. E. Larkum, T. Nevian, M. Sandler, A. Polsky, J. Schiller, *Science* **325**, 756–760 (2009).
21. J. J. Zhu, *J. Physiol.* **526**, 571–587 (2000).
22. J. Schiller, Y. Schiller, G. Stuart, B. Sakmann, *J. Physiol.* **505**, 605–616 (1997).
23. M. L. Hines, N. T. Carnevale, *Neural Comput.* **9**, 1179–1209 (1997).
24. M. London, M. Häusser, *Annu. Rev. Neurosci.* **28**, 503–532 (2005).
25. A. Polsky, B. W. Mel, J. Schiller, *Nat. Neurosci.* **7**, 621–627 (2004).
26. A. Losonczy, J. C. Magee, *Neuron* **50**, 291–307 (2006).
27. E. Boldog *et al.*, *Nat. Neurosci.* **21**, 1185–1195 (2018).
28. A. Gidon, I. Segev, *Neuron* **75**, 330–341 (2012).
29. A. T. Gulledge, G. J. Stuart, *Neuron* **37**, 299–309 (2003).
30. G. M. Shepherd, R. K. Brayton, *Neuroscience* **21**, 151–165 (1987).
31. M. Minsky, S. A. Papert, *Perceptrons: An Introduction to Computational Geometry* (MIT Press, 1969).
32. F. Rosenblatt, *The Perceptron, a Perceiving and Recognizing Automaton: (Project Para)* (Cornell Aeronautical Laboratory, 1957).
33. G. Eyal *et al.*, *Front. Cell. Neurosci.* **12**, 181 (2018).
34. P. Poirazi, T. Brannon, B. W. Mel, *Neuron* **37**, 989–999 (2003).
35. G. Testa-Silva, S. Honnuraiah, C. French, J. King, K. Drummond, L. M. Palmer, G. J. Stuart, "NMDA spikes in human neocortex," program no. 463.12, *2018 Neuroscience Meeting Planner*, Society for Neuroscience, San Diego, CA, 3 to 7 November 2018.
36. A. Gidon *et al.*, Dendritic action potentials and computation in human layer 2/3 cortical neurons. Zenodo (2020); https://doi.org/10.5281/zenodo.3530043.

SUPPLEMENTARY MATERIALS

science.sciencemag.org/content/367/6473/83/suppl/DC1
Materials and Methods
Figs. S1 to S12
Tables S1 and S2
References (*37–51*)

View/request a protocol for this paper from *Bio-protocol*.

Science

Dendritic action potentials and computation in human layer 2/3 cortical neurons

Albert Gidon, Timothy Adam Zolnik, Pawel Fidzinski, Felix Bolduan, Athanasia Papoutsi, Panayiota Poirazi, Martin Holtkamp, Imre Vida and Matthew Evan Larkum

Human dendrites are special
　　　A special developmental program in the human brain drives the disproportionate thickening of cortical layer 2/3. This suggests that the expansion of layer 2/3, along with its numerous neurons and their large dendrites, may contribute to what makes us human. Gidon *et al.* thus investigated the dendritic physiology of layer 2/3 pyramidal neurons in slices taken from surgically resected brain tissue in epilepsy patients. Dual somatodendritic recordings revealed previously unknown classes of action potentials in the dendrites of these neurons, which make their activity far more complex than has been previously thought. These action potentials allow single neurons to solve two long-standing computational problems in neuroscience that were considered to require multilayer neural networks.
　　　Science, this issue p. 83

ARTICLE TOOLS	http://science.sciencemag.org/content/367/6473/83
SUPPLEMENTARY MATERIALS	http://science.sciencemag.org/content/suppl/2019/12/30/367.6473.83.DC1
REFERENCES	This article cites 47 articles, 12 of which you can access for free http://science.sciencemag.org/content/367/6473/83#BIBL
PERMISSIONS	http://www.sciencemag.org/help/reprints-and-permissions

Use of this article is subject to the Terms of Service